Looking inside a microwave oven for continuous flow heating by IR Thermography

GENNARO CUCCURULLO, LAURA GIORDANO
Department of Industrial Engineering
University of Salerno
Via Giovanni Paolo II n. 132, 84084 Fisciano
ITALY
cuccuru@unisa.it, lagiordano@unisa.ithttp://www.unisa.it/docenti/gennarocuccurullo/index

GIACOMO VICCIONE
Department of Civil Engineering
University of Salerno
Via Giovanni Paolo II n. 132, 84084 Fisciano, Italy
ITALY
gviccion@unisa.ithttp://www.unisa.it/docenti/giacomoviccione/index

A first attempt for on-line quantitative IR-thermography temperature readout has been performedinside an illuminated microwave oven.The main aim was to feature bulk temperature profiles in laminar pipe flow.The proposed procedure is intended to overcome the well-known difficulties connected with temperature retrieval while microwave (MW) heating occurs, whilepromotinghighspatial resolutions.In fact, temperature measurements are usually taken onto few points by means of fiberoptic probes. Such an approach is often inadequate for properly controlling the process at hand, as strongly uneven spatial distribution of the temperature fieldis expected as a consequence of the electromagnetic distribution inside the cavity. Considering theoretical results already obtainedby the authors, a linear distribution of the bulk temperature wasrealized for high water flow rates occurring in a circular pipe exposed to MW heating. Such an occurrence allowed aproper preliminary calibration basedon which, a procedurefor processing infrared imagesin real time is proposed. Experimentalresults related to two temperature levels, namely 40 and 50 °C, and two flow rates, that is 4 and 5.7 g/s, are reported. Experimental values of bulk temperature werecompared with numerical results obtained by applying a 3D FEM model, developed by the authors, accounting for constant dielectric and thermal properties. A quite satisfying agreement between experimental and numerical datawasfound, retrieving better results with increasing flow rates.

Key-Words: -Microwave heating of liquids, Maxwell's equations, Numerical modelling, FEM, CFD, Comsolmultiphysics, Experimental validation, Infrared thermography.

1 Introduction

Thermal treatment of liquids using microwaves (MW) is an effective, low-cost way of processing. Warming takes place all over the exposed mass as moleculae are locally excited, in contrast withconventional methods where heating is transferred throughconvection and heat conduction from the surface to the inner side.

Nowadays, it is widely recognized that attracting advantages of MW application over conventional heating techniques essentially consist in minor periods needed for the processing, higher energy efficiency, absence of contaminants released in the atmosphere or more in general in the environment. The latteraspect is becoming particularly attractive, as for instance proved by specific investmentsset under the Horizon 2020 program, aimed to the reduction of pollutant sources in the Mediterranean.

For a comprehensive discussion of heat and mass transfer processing in MW heating refer to Metaxas and Meredit [1] and Saltiel and Datta[2].

While there is a large amount of papers dealing with numerical modelling of MW heating of solid substances [3], [4], [5],[6],[7],[8]; [9], [10], minor attention seems to have beenpaid to liquids (see for instance [11], [12], [13]), despite a well established interest into thermally treating them[14], [15], e.g., for heating, drying, melting, pasteurizing, sterilizing, etc.First attempts have been made into modelling the MW power transferring by theoretical models, i.e. based on the Lambert's law.

ISBN: 978-960-474-377-3

Nevertheless, such an assumption is not valid for small samples (that is the case at hand) in which expected EM spatial gradients must be derived by solving Maxwell's equations. Concerning liquids, a numerical approach is needed, especially when such a set of equations is coupled with convective heat transfer and liquid momentum equations. Not to mention, the case in which dielectric properties are assumed to be temperature dependent.

Among the others (QuickWave-3D, MEFiSTo-3D, Microwave studio and so on), there are basically two main commercial models capable of solving thermal treatment by MWs: ANSYS Multiphysics [16] and COMSOL Multiphysics [13], [17], [18], [19].A comparison betweenANSYS and COMSOL models is proposed in [12].

The correctness of the adopted numerical procedure should be checked by experimental validation of the results. Still, there are few cases of literature where such a requirement is fulfilled (see for instance [20], [21]).Although the experimental approachprovides evidencefor the matter being investigated, satisfactoryexperimentation may be unpractical as a greatamount of tests and an adequate number of sampling points are usually necessaryto obtain reliable results since scale-up analysis is not allowed.

Measurement ofinterestingparameters is not an easy task as the measuring devices may interfere withthe electromagnetic field and with theflow motion in continuous processes.To tackle with the latter issue, appropriate procedures for field measurement have been long established in the past. Mamouni and co-workers [22], [23] proposed the correlation microwave thermography technique (CMWT) for the accurate description of thermal distribution on material's surfaces. In [24] kidney-bladder system pathologies are assessed by correlating MW radiometry with temperature measurementstaken by fiberoptic probes. Cuccurullo et al proposed an innovative procedure for real time controlling apple drying based on IR thermography, [25].

Here, a first attemptis madefor a quantitative infrared thermography temperature readout to describe in real time temperature field inside an illuminated MW cavity.

Given the fact that temperature measurements are usually taken onto few points by means of fiberoptic probes, the proposed procedure is intended to promote higher resolutions than standard's. Such anapproach is needed, asstrongly uneven spatial distribution of the temperature field, produced by MW application, are expected. Consideringthe theoretical results obtained in [18], a linear distribution of temperature can be assumed for highflow rates, flowing in a circular pipe exposed to MWs. On such assumption, a procedure, based on the processing of infrared images taken inside the oven and able to provide the water bulk temperature fieldalong the pipe, is proposed.

2 Materials and methods

2.1 Experimental setup

Experiments were performed in a microwave pilot plant, Figure 1, intended for general purposes in order to encompass different loads, i.e. different materials and samples distributions, weight, size. Microwaves were generated by a magnetron rated at 2 kW nominal power output and operating at a frequency of 2.4 GHz. A rectangular WR340 waveguide connects the magnetron to the cavity. Microwaves illuminated an insulated metallic cubic chamber (0.9 m side length) housing the pyrex(MW transparent) glass applicator pipe (8 mm inner diameter, 1.5 mm thick) carrying water continuous flow to be heated.

The inner chamber walls were insulated by polystyrene slabs black painted. The pipe was placed inside the chamber in such a way that its longitudinal axis lied down along a plane symmetrical both for geometry and load conditions. Such a choice was realized having in mind to suitably reduce computational efforts, as next explained.

A centrifugal fan facilitated the air removal by forcing external air into the cavity; the renewal air flow was kept constant throughout the experiments in order to stabilize the heat transfer coefficient between the pipe and the environment. The channel feeding the external air flow was equipped with an electric heater controlled by the feedback from a thermocouple in order to realize a fixed temperature level inside the illuminated chamber, that is 23°C.

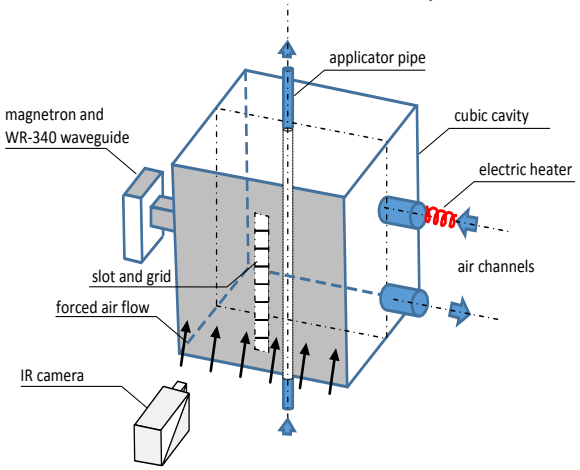

Fig.1. Sketch of the available MW pilot plant

ISBN: 978-960-474-377-3

2.2 The numerical procedure

A 3D finite element method (FEM) model was developed in COMSOL v4.4environment [26]. The software allows coupling electromagnetic, flow and thermal problems to predict temperature distribution in the moving fluid. The need of considering coupled physics and thus a general solution, arises by noting that, due to the geometry at hand, no simplified heating distributions can be assumed (i.e. the ones based on Lambert Law's) [27].

The electric field distribution $\underline{E}$ in the microwave cavity, both for air and for the applicator pipe carrying the fluid under process, is determined by imposing

$$\nabla\times\left(\frac{1}{\mu_r}\nabla\times\underline{E}\right)-k_0^2\left(\varepsilon_r-\frac{i\sigma}{\omega\varepsilon_0}\right)\underline{E}=\underline{0} \qquad (1)$$

where$\varepsilon_r$and $\mu_r$are the relative permittivity and permeability respectively,assumed to be constant, ω is the angular wave frequency, k_0 is the wavenumber in vacuum, and σ is the electric conductivity.

Assuming negligible resistive material losses, inner walls can be assumed as perfect electric conductors, that is, $\underline{n}\times\underline{E}=\underline{0}$, for the waveguide and the cavity surfaces, being $\underline{n}$ the local normal vector.

Continuity boundary conditions were set by default for all the interfaces between the confining domains, that is, the pipe, the cavity, and the waveguide. Such condition may be expressed as

$$\underline{n}\times(\underline{E}_i-\underline{E}_j)=\underline{0} \qquad (2)$$

being i and j the neighbouring discrete facets, sharing the interface at hand.

Due to the symmetry of the problem, and load conditions around the plane crossing vertically the oven, the waveguide, and the pipe the model is reduced to one-half of the device, yielding a more accuracy in the calculation. The condition of perfect magnetic conductor was applied for the surfaces yielding on the symmetry plane:

$$\underline{n}\times\underline{H}=\underline{0} \qquad (3)$$

$\underline{H}$ being the magnetic field, which has to be therefore parallel to the local normal vector $\underline{n}$ on the symmetry plane.

Temperature distribution is determined for fully developed Newtonian fluid in laminar motion, considering constant flow properties; in such hypotheses, the energy balance reduces to

$$\rho c_p U\frac{\partial T}{\partial X}=k\nabla^2T+U_{gen} \qquad (4)$$

where T is the temperature, ρ is the fluid density, c_p is the specific heat, k is the thermal conductivity, X is the axial coordinate, $U(R)=2U_{av}(1-4\cdot R^2/D_i^2)$ is the axial Poiseille velocity profile, D_i being the internal pipe diameter and R the radial coordinate,U_{av} is the average velocity on the cross section being considered; U_{gen} is the specific heat generation, i.e. the "electromagnetic power loss density" (W/m^3) resulting from the numerical solution of the EM problem. The power-generation term realizes the coupling of the EM field with the energy balance equation.It represents the "heat source" term:

$$U_{gen}(X,Y,Z)=\frac{1}{2}\omega\varepsilon_0\varepsilon''\left|\underline{E(X,Y,Z)}\right|^2 \qquad (5)$$

beingε_0 is the free-space permittivity and ε" is the relative dielectric loss of the material.

2.3.Temperature readout procedure

The presence of the grid is a major obstacle wishing to perform temperature-readout when looking inside the illuminated cavity. The focus is set on the applicator pipe, while the instantaneous field of view (IFOV) of the radiometer in use may well find the hot spots corresponding to the pipe below the grid. Nevertheless, the radiometer does not accurately measure pipe temperatures due to the slit response function (SRF) effect. Because of the SRF, the object's temperature drops as the distance from the radiometerincreases. The latter was set in order to encompass in the IR image the maximum pipe extension compliant with the available slot-window carrying the grid.On the other hand, the need of getting as close to the target as possible, in the respect of the minimum focal distance.

A preliminary calibration and a suitable procedure have been then adopted. First, the glass-pipe, the grid and the cavity walls have been coated with a high emissivity black paint whose value was measured to be $\varepsilon = 0.95$. Then the following configurations have been considered:

(a)the "test configuration", i.e. the applicator-pipe carrying the fluid @ fixed inlet temperature.

(b)the "reference configuration", i.e. a polystyrene slab placed inside the cavity in order to blind the pipe to the camera view. The slab was black painted to realize an emissivity of0.95 and its temperature, T_{slab}, was measured by four fiberoptic probes.

ISBN: 978-960-474-377-3

For both (a) and (b) configurations, neglecting the atmosphere contribution, the fundamental equation of IR thermography relates the spectral radiant power incident on the radiometerto the radiance leaving the surface under consideration. For the case at hand, the attenuation due to the grid must be taken into account. The radiance coming from the inner walls is attenuated by a factor τ, defined in what follows as "grid transmissivity", which accounts for the SRF grid effect. The latter parameter depends on both the geometry and the temperature level involved. Additionally, the radiometer receives both the radiance reflected from the external surroundings ambient to the grid and the emission by the grid itself. The inner and outer surrounding environments are considered as a blackbodies @ uniform temperatures T_i and T_o, respectively. Finally, the radiometric signal weighted over the sensitivity band by the spectral response of the detection system, including the detector sensitivity, the transmissivity of the optical device and amplification by the electronics, is proportional tothe target radiance as follows:

$$I(T_{\text{slab}}^{\text{app}}) = \tau[\varepsilon I(T_{\text{slab}})+(1-\varepsilon)I(T_i)]+(1-\tau)[\varepsilon I(T_{\text{grid}})+(1-\varepsilon) I(T_o)] \quad (6)$$

$$I(T_{\text{pipe}}^{\text{app}}) = \tau[\varepsilon I(T_{\text{pipe}})+(1-\varepsilon)I(T_i)]+(1-\tau)[\varepsilon I(T_{\text{grid}})+(1-\varepsilon) I(T_o)] \quad (7)$$

where I is the blackbody Planck's function, evaluated at a suitable wavelength, within the radiometer spectral sensitivity window, λ^+.With reference to the radiometer in use, this latter parameter turns out to be $\lambda^+ = 11.5$ μm as obtained by instrument calibration data.

It is worth to recall that the apparent temperatures (on left side of above eqs. (6) and (7)) are the surface ones given by an equivalent blackbody as seen by the IR equipment, both for the pipe and the polystyrene slab. The calibration curve related to the specific radiometerallows the retrieval of apparent temperatures,see next paragraph. The exogen contributions due to both the reflections arising from inner and outer walls clearly appear. Only the former contribution is attenuated by the presence of the grid. The last contribution represents the reinforcement due to the grid emission.

Subtracting the two previous equations (6) and (7), the contribution due to the grid cancels, thus yielding:

$$\varepsilon\tau = \frac{I(T_{\text{pipe}}^{\text{app}}) - I(T_{\text{slab}}^{\text{app}})}{I(T_{\text{pipe}}) - I(T_{\text{slab}})} \quad (8)$$

Most commonly in thermography, the subtraction (Figure 2) of images related to configurations (a) and (b) produces the further benefit of cancelling the grid established uneven temperature distribution,which probably stems from eddy currents occurrence.

In order to explicit the dependence of the radiance on the temperature, the Plank's law can be rearranged, considering that

$$\frac{\mathrm{d}I_{b,\lambda} / I_{b,\lambda}}{\mathrm{d}T / T} = \frac{C_2}{\lambda T}\frac{e^{\frac{C_2}{\lambda T}}}{e^{\frac{C_2}{\lambda T}} - 1} \approx \frac{C_2}{\lambda T} \quad (9)$$

C_2 = 14390 μm Kbeing the 2nd radiation constant. The approximation due to Wien which is recalled in the last passage leads to an error less that 1% if the wavelengths are not greater than 2.5 λ_{max}, λ_{max} being the wavelength for which the maximum emission is attained at the actual temperature. These conditions are fully recovered for the case at hand. In view of the previous expression, if one assumes $I \approx T^n$, it is readily recovered that $n \approx 5\ \lambda_{max}/\ \lambda^+$. Finally, the last expression can be set as:

$$\varepsilon\tau = \frac{\left(T_{\text{pipe}}^{\text{app}}\right)^{n(T_{\text{pipe}}^{\text{app}})} - \left(T_{\text{slab}}^{\text{app}}\right)^{n(T_{\text{slab}}^{\text{app}})}}{\left(T_{\text{pipe}}\right)^{n(T_{\text{pipe}})} - \left(T_{\text{slab}}\right)^{n(T_{\text{slab}})}} \quad (10)$$

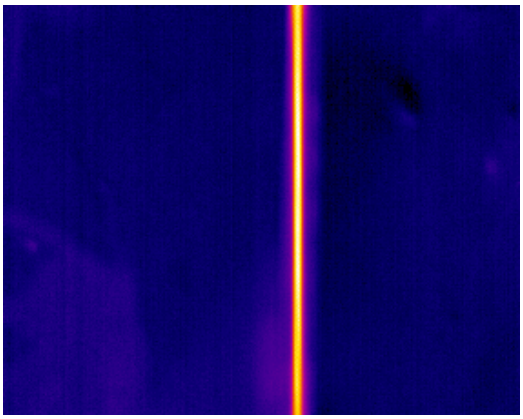

Fig. 2. Net apparent applicator pipe temperatures

ISBN: 978-960-474-377-3

The notation resembles that the index n depends on the temperature itself. In view of this equation, provided the apparent temperatures are known via IR thermography and the slab temperature via the fiber optic probes, the function $\varepsilon\tau$ is required in order to infer the pipe temperature. The calibration is then intended to determine the $\varepsilon\tau$ as function of both geometry and temperature levels.The calibration is carried on as follows. First, the water flow discharge was kept as high as a linear temperature increase could be experienced for the bulk temperature of the flowing fluid [18]. Thus, measuring the fluid inlet and outlet temperatures by thermocouples placed externally to the illuminated cavity, allowed to know the true bulk water temperature along the longitudinal x axis of the pipe, $T_{\text{pipe}}^{\text{bulk}}(x)$. On the other hand, the need of realizing high flow rates determined temperature increases contained within ΔT_{bulk}= 2.6°C and thus allowed to fix the corresponding temperature level for the test at hand.Seven inlet temperatures, namely T_{inlet} = 40, 50, 55, 60, 65, 70 and 75 °C, were considered which covered the temperature range involved in the successive experimental tests.

Assuming that the surface pipe temperature closely approaches the fluid bulk temperature $T_{\text{pipe}}(x) \cong T_{\text{pipe}}^{\text{bulk}}(x)$, knowing the apparent temperatures via IR thermography and measuring the slab temperature, eq. (10) allows to evaluate $\varepsilon\tau$ as function of the axial coordinate along the tube longitudinal axis (x) in correspondence of the sevenpreset true temperature levels, T = (T_{inlet}+ T_{outlet})/2.

In particular, since the relative-shape of the $\varepsilon\tau$-function along the axial coordinate appeared to be the same but its level was increasing with temperature level, the $\varepsilon\tau$-function was sought as $\varepsilon\tau(x,T) = f_1(x) + f_2(T)$.

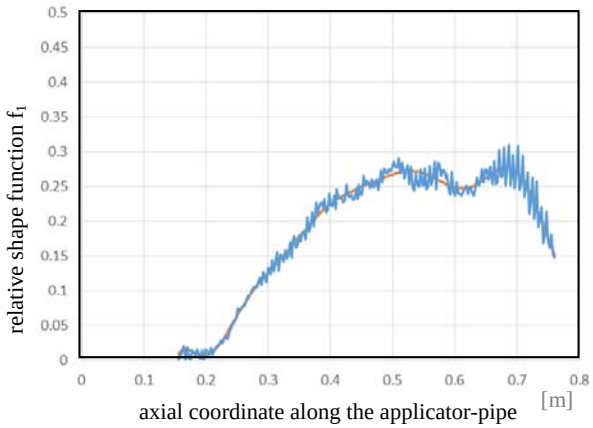

Fig.3. Measured and interpolated relative shape-function f_1.

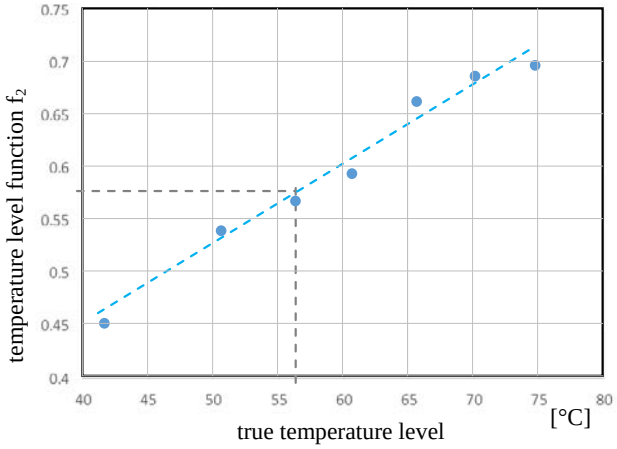

Fig 4. Temperature level function f_2 obtained with a linear regression.

The function f_1 was recovered by averaging the seven relative shapes and turned out to be well approximated (R^2 = 0.996) by a 10-th order polynomial, Figure3, while $f_2$resulted to be almost linear with temperature, Figure4, the maximum relative error being contained within 3%, i.e. R^2 = 0.974. As an example, the measured $\varepsilon\tau$–function @ 55°C is compared with the corresponding one based on the above interpolating structure in Figure5: the satisfying agreement is witnessed by an average relative error contained within 1.68%.

Applying the same procedure to the remaining selected temperature levels similarly shows that measured and reconstructed curves fairly agree, thus showing that the procedure at hand fits well the experimental data. The maximum among the average relative errors corresponding to the selected temperature levels is 2.3 %.

The knowledge of the $\varepsilon\tau$ function enables the IR image processing described in the following section.

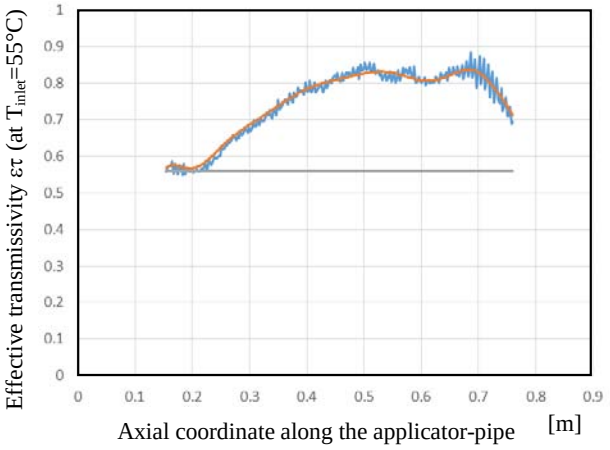

Fig. 5. The reconstructed and measured true

ISBN: 978-960-474-377-3

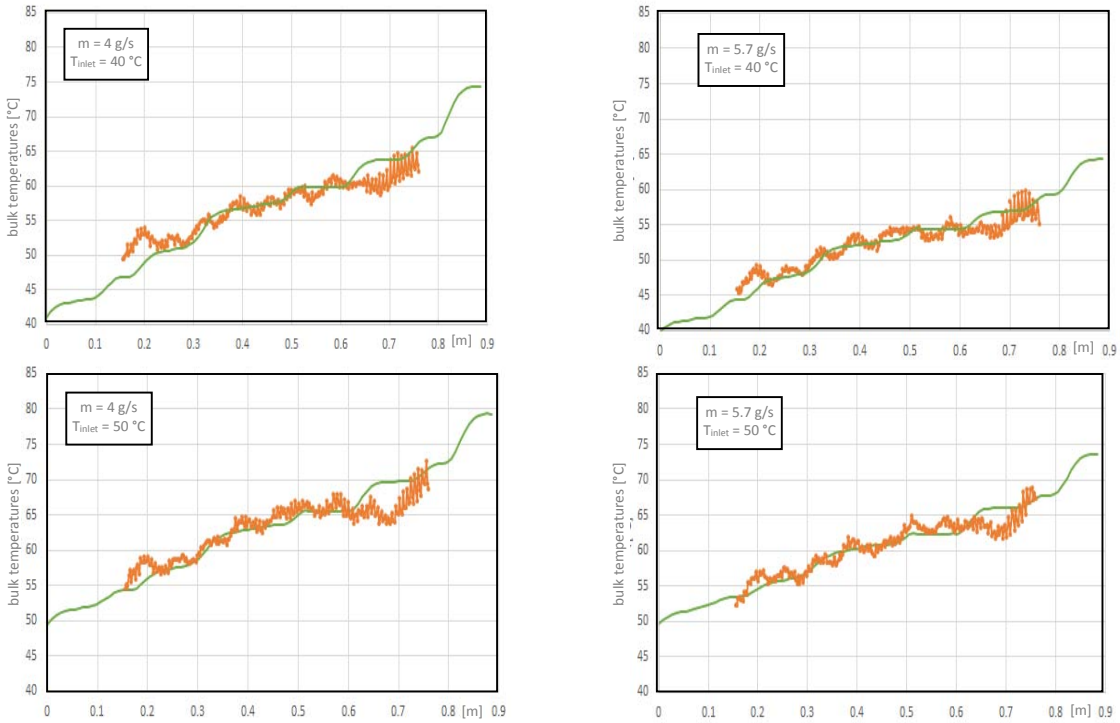

Fig.6. Numerical (green lines) and experimental bulk temperatures (orange dotted lines) for inlet temperaturesT_{inlet}= 40 and 50 °C, and two flow rates m = 4 and 5.7 g/s.

temperature profiles @ T_{inlet}= 55°C.

2.4Image processing

In view of the discussion previously presented, tests related to configuration (a) were performed. Provided steady conditions were attained, an image sequence at the rate of 10 images per second wastaken for two seconds. Since frames in time sequence differ only in the distribution of random noise, twenty frames were averaged to form a single image with noise variance reduced proportionally to the sequence length. Performing a horizontal scan of the formed image, the maximum apparent temperature for each row was extracted, identifying in such way the proper pipe longitudinal apparent temperature.

In a similar fashion, processing an image sequence related to configuration (b), the apparent slab temperatures were extracted in correspondence of the pixels selected by processing configuration (a). Finally, eq. (10)was solved for each point *x*along the pipe axis in terms of the unknown true pipe temperatureT_{pipe}, T_{slab}being measured by the fiberoptic probes.

3 Results and discussion

Experimental curves and the corresponding numerical ones resulting from data reduction are reported in Figure 6. Two temperature values of inlet temperature, namely 40 and 50 °C, and two flow rates, that is 4 and 5.7 g/s, were considered. Thermal and dielectric properties used during the numerical simulations were evaluated in correspondence of the average temperature of the flowing liquid resulting from the experiments. The input power feeding the numerical model was chosen such that the total power loss was equal to the one resulting from the experiments by calorimetric computations.

A quite satisfying agreement between experimental and numericaldata exists, at least in terms of qualitative behaviour: the uneven temperature distribution which is due, in turn, to the EM field patterns, seems to be recovered. The corresponding RMSE values, as shown in Table 1, confirm that increasing the flow rates increases the accuracy of the prediction. This occurrence is expected since the uneven temperature distribution inside pipe section is reduced with increasing the fluid average speed[18], both because of the increasing frequency effect of the forcing EM fieldand of the increased velocity which compensates the augmented energy concentration in the region nearby the longitudinal axis of the pipe.Therefore, bulk temperature values are closely approached by the wall temperature in each section, as supposed in advance.

ISBN: 978-960-474-377-3

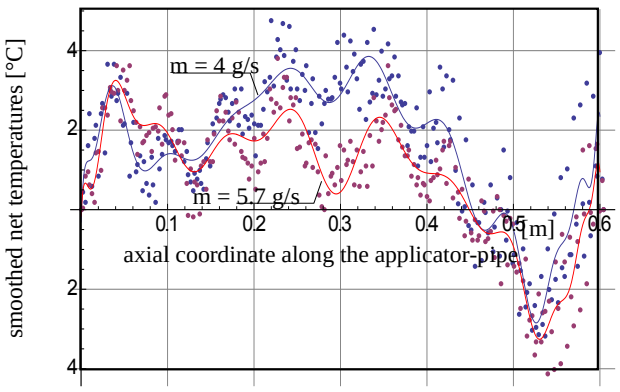

Fig.7. Polynomial fitting (continuous lines) of net temperatures data for m=4g/s and 5.7g/s, taking T_{inlet} = 50 °C.

Mass flow rate m[g/s]	T_{inlet} [°C]	RMSE [°C]
4	40	5.5
5.7	40	4.1
4	50	4.6
5.7	50	3.6

Table 1. RMSE of bulk temperatures for different mass flow rates and temperature levels.

A further proof of the reliability of the experimental tests may be deduced by generating a symbolic representation (see Figure 7), giving the best fit of experimental temperature profiles evaluated in excess with respect to the local bulk temperatures corresponding to the uniform heat generation solution [17]. In fact, this “move” allows evidencing the expected increasing attenuation and delay of the net temperature profiles because of the increased flow rates.

4 Conclusion

A new experimental procedure for estimating the bulk temperature distribution in water flowing in a glass-pipe, subjected to microwaves, has been proposed. Infrared thermography allowed to obtain high-resolution thermal maps in real time. The presence of the grid between the pipe and the radiometerrequired a suitable calibration in order to evaluate the ετ-function along the pipe, before performing the experimental tests.

Two temperature levels, namely 40 and 50 °C, and two flow rates, that is 4 and 5.7 g/s, were considered. The experimental values of bulk temperature were compared with resultsobtained by solving a FEM model, which accounts for constant dielectric and thermal properties. A quite satisfying agreement between experimental and numerical data was found, with a better prediction for higher flow rates.

A wider flow range has be explored and the effect of temperature dependent fluid properties will be implemented in the numerical model in order to improve the theoretical prediction of the experimental results.

References:

[1] A.C. Metaxas, R.J. Meridith, Industrial Microwave Heating, *Peter Peregrinus*, London, 1983.

[2] C. Saltiel, A. Datta, Heat and mass transfer in microwave processing, *Adv. Heat Transfer*, 30, 1997, pp. 1–94.

[3] K.G. Ayappa, H.T. Davis, E. A. Davis, J.Gordon, 1992, Two-Dimensional Finite Element Analysis of Microwave Heating, AiChE Journal, 38, 10, pp. 1577-1592.

[4] Y.E Lin,., R.C. Anantheswaran and V.M. Puri, 1995, Finite Element Analysis of Microwave Heating of Solid Foods,*Journal of Food Engineering*, 25, pp. 85-112.

[5] L. Zhou, V.M. Puri, R.C. Anantheswaran, G. Yeh, 1995, Finite element modeling of heat and mass transfer in food materials during microwave heating — Model development and validation, *Journal of Food Engineering*, 25, 4, pp. 509–529

[6] H. Zhao, I.W. Turner, 2000, The use of a coupled computational model for studying the microwave heating of wood, *Appl. Math. Modeling*, 24, pp. 183–197.

[7] M.E.C. Oliveira, A.S. Franca, 2002, Microwave Heating of Foodstuffs, *Journal of Food Engineering*, 53, pp.347-359.

[8] R.B.Pandit, S. Prasad, 2003, Finite element analysis of microwave heating of potato--transient temperature profiles, *Journal of Food Engineering*, 60, 2, pp. 193-202.

[9] V.R. Romano, F. Marra, U. Tammaro, 2005, Modelling of microwave heating of foodstuff: study on the influence of sample dimensions with a FEM approach, *Journal of Food Engineering*, 71, pp. 233-241.

[10] L. Dubcova, P. Solin, J. Cerveny, P. Kus, 2010, Space and Time Adaptive Two-Mesh hp-Finite Element Method for Transient Microwave

ISBN: 978-960-474-377-3

Heating Problems, *Electromagnetics*, 30, pp. 23-40.

[11] T. Yousefi, S.A. Mousavi, M.Z. Saghir, B. Farahbakhsh, 2013, An investigation on the microwave heating of flowing water: A numerical study, International Journal of Thermal Sciences, pp. 118-127.

[12] D. Salvi, DorinBoldor, J. Ortego, G. M. Aita, C. M. Sabliov, 2010, Numerical Modeling of Continuous Flow Microwave Heating: A Critical Comparison of COMSOL and ANSYS, *Journal of Microwave Power and Electromagnetic Energy*, 44(4), pp. 187-197.

[13] P. D. Muley, D. Boldor, 2012, Multiphysics Numerical Modeling of the Continuous Flow Microwave-Assisted Transesterification Process, *Journal of Microwave Power and Electromagnetic Energy*, 46 (3), pp. 139-162.

[14] I. Sierra, C. Vidal-Valverde, A. Olano, 1999, The effects of continuous flowmicrowave treatment and conventional heating on the nutritional value of milk as shown by influence on vitamin B1 retention, European *Food Research and Technology*, 209(5), pp. 352–354.

[15] S. Tajchakavit, H. S. Ramaswamy, P. Fustier, 1998, Enhanced destruction of spoilage microorganisms in apple juice during continuous flow microwave heating," *Food Research International*, 31(10), pp. 713–722.

[16] C. M. Sabliov, , D. A. Salvi, D. Boldor, 2007, High frequency electromagnetism, heat transfer and fluid flow coupling in ANSYS multiphysics, *Journal of Microwave Power & Electromagnetic Energy*. 41(4), pp. 5-17.

[17] G. Cuccurullo, L. Giordano, G. Viccione, 2014, A fast and accurate hybrid model for simulating continuous pipe flow microwave heating of liquids, *International Journal of Mechanics*, 8(1), pp. 45–52.

[18] G. Cuccurullo, L. Giordano, G. Viccione, 2013, An analytical approximation for continuous flow microwave heating of liquids, *Advances in Mechanical Engineering*.

[19] G. Cuccurullo, L. Giordano, G. Viccione, 2013, Toward an Improved Hybrid Model for Simulating Continuous Flow Microwave Heating of Water. In:*Recent Advances in Mechanics, Fluids, Heat, Elasticity and Electromagnetic Fields*,Venezia, pp.182-189.

[20] W. Cha-um, P. Rattanadecho, W. Pakdee, 2009, Experimental and Numerical Analysis of Microwave Heating of Water and Oil Using a Rectangular Wave Guide:Influence of Sample Sizes, Positions, and Microwave Power, *Food Bioprocess Technol*, 4, pp. 544–558.

[21] W. Klinbun, P. Rattanadecho, W. Pakdee, 2011, Microwave heating of saturated packed bed using a rectangular waveguide (TE10 mode): Influence of particle size, sample dimension, frequency, and placement inside the guide, International Journal of Heat and Mass Transfer, 54, 1763-1774.

[22] A. Mamouni, J. C. Van De Velde, Y. Leroy, 1981, New correlation radiometer for microwave thermography, *ibid*., 1981, 17, pp. 554-555.

[23] A. Mamouni, Y. Leroy, J. C. Van DdeVelde, L. Bellarbi, 1983, Introduction to correlation microwave thermography, *J. Microwave Power*, 18, pp. 285–293.

[24] S. K. Jacobsen, Ø. Klemetsen,Y. Birkelund, 2012,Vesicoureteral reflux in young children: a study of radiometric thermometry as detection modality using an ex vivo porcine model, *Physics in Medicine and Biology*, 57(17), pp. 5557 – 5573.

[25] G. Cuccurullo, L. Giordano, D. Albanese, L.Cinquanta, M. Di Matteo, 2012, Infrared thermography assisted control for apples microwave drying, *Journal of Food Engineering*,Elsevier, 112(4), pp. 319 – 325

[26] COMSOL Multiphysics Version 4.4 User Guide, December 2013.

[27] A. Datta, H. Prosetya, and W. Hu, 1992, Mathematical modeling of batch heating of liquids in a microwave cavity,*Journal of Microwave Power and Electromagnetic Energy*, 27(1), pp. 38–48.